IJCARS manuscript No.
(will be inserted by the editor)

Multi-modal 3D ultrasound and CT in image-guided spinal surgery: public database and new registration algorithms

Nima Masoumi · Clyde J. Belasso · M. Omair Ahmad · Habib Benali · Yiming Xiao · Hassan Rivaz

Received: date / Accepted: date

Abstract
Purpose:Accurate multi-modal registration of intraoperative ultrasound (US) and preoperative computed tomography (CT) is a challenging problem. Construction of public datasets of US and CT images can accelerate the development of such image registration techniques. This can help ensure the accuracy and safety of spinal surgeries using image-guided surgery (IGS) systems where an image registration is employed. In addition, we present two algorithms to register US and CT images.
Methods: We present three different datasets of vertebrae with corresponding CT, US, and simulated US images. For each of the two latter datasets, we also provide 16 landmark pairs of matching structures between the CT and US images and performed fiducial registration to acquire a silver standard for assessing image registration. Besides, we proposed two patch-based rigid image registration algorithms, one based on normalized cross correlation (NCC) and the other based on correlation ratio (CR) to register misaligned CT and US images.
Results: The CT and corresponding US images of the proposed database were pre-processed and misaligned with different error intervals, resulting in 6000 registration problems solved using both NCC and CR methods. Our results show that the methods were successful in aligning the preprocessed CT and US images by decreasing the warping index.
Conclusions: The database provides a resource for evaluating image registration techniques. The simulated data have two applications. First, they provide the gold standard ground–truth which is difficult to obtain with ex–vivo and in–vivo data for validating US–CT registration methods. Second, the simulated US images can be used to validate real–time US simulation methods. Besides, the proposed image registration techniques can be useful for developing methods in clinical application.

Keywords image registration · ultrasound simulation · vertebrae · dataset

N. Masoumi
PERFORM Centre, Concordia University, Montreal, Canada
Department of Electrical and Computer Engineering, Concordia University, Montreal, Canada
E-mail: n_masoum@encs.concordia.ca

C. J. Belasso
Department of Electrical and Computer Engineering, Concordia University, Montreal, Canada
E-mail: c_belas@encs.concordia.ca

M. O. Ahmad
Department of Electrical and Computer Engineering Concordia University Montreal, Canada
E-mail: omair@ece.concordia.ca

H. Benali
PERFORM Centre, Concordia University, Montreal, Canada
Department of Electrical and Computer Engineering, Concordia University, Montreal, Canada
E-mail: habib.benali@concordia.ca

Y. Xiao
Department of Computer Science and Software Engineering, Concordia University, Montreal, Canada
E-mail: yiming.xiao@concordia.ca

H. Rivaz
PERFORM Centre, Concordia University, Montreal, Canada
Department of Electrical and Computer Engineering, Concordia University, Montreal, Canada
E-mail: hrivaz@ece.concordia.ca

1 Introduction

Intraoperative ultrasound (US) is non-invasive, renders real-time images of soft tissue, and has been used in image-guided surgery (IGS) to help increase the accuracy of surgical interventions [1,2]. Acquiring intraoperative US for IGS is beneficial in multiple types of spinal surgeries: for lumbar vertebrae spinal fusion surgery for degenerative disc disease (DDD), for canine spinal cord surgery (mostly in the middle vertebrae) for interventional disc disease (IVDD), and for spinal surgeries that stabilize vertebral fractures [3,4].

Prior to a spinal surgery, computed tomography (CT) images are acquired pre-operatively to plan the intervention. To help guide the surgical procedure during surgery, intra-operative US images corresponding to the pre-operative CT images can help increase the accuracy of the surgery. Image registration in IGS is required because the intra-operative US must be spatially aligned with the pre-operative image so that the image fusion algorithm can be applied to integrate the information during the operation. Simulation of the US image from the pre-operative image can increase the accuracy of this multi-modal image registration [5].

Current US simulation techniques are divided into two categories: ray-based methods and wave-based methods [6,7]. Ray-based methods are quicker in computation time but they do not provide realistic images whereas wave-based methods are more realistic but lack US specific artifacts such as shadowing [8]. Alternatively, wave-based methods, for instance Field II simulation software, can be used as a ground-truth for other simulation techniques at the expense of having a greater computation time [9].

Previous work has developed multi-modal image registration algorithms to align the CT-US and CT-simulated US images [10,11]. However, the following shortcomings exist in the implementation and validation of their methods. First, the utilized datasets are not publicly available. Employing a publicly available data can provide researchers a valuable information to further compare their methods with the existing ones. Second, the implementation of single-scale methods restrict performing registration on larger initial misalignment. Third, by assuming that the rigid registration is sufficient to compensate the initial misalignment, given the 6 degree of freedom (DOF), the resolution of images, and the machine precision, exhaustive image registrations may require to be performed for each range of initial misalignment. This can reveal valuable information about the robustness and applicability of method in real applications.

Following the success of our database of US and magnetic resonance (MR) images [12], we created a database of CT scans and corresponding US images, and proposed a simple and realistic wave-based US simulation method to simulate the US images from the CT images. In the first part of the database, the US from The Cancer Genome Atlas Sarcoma of the three patients' lumbar vertebrae (TCGA-SARC) [13, 14] were simulated from their CT images. In the second part of the database, the CT scan, the spatially tracked US, and the simulated US of the canine thoracic and cervical vertebrae phantom are provided. In the third part of the database, the CT scan, the spatially tracked US, and the simulated US of the lamb lumbar vertebrae are provided. For each of the two latter datasets, we provided 16 landmarks of analogous structures in the CT and US images and performed fiducial registration to acquire a silver standard ground-truth of the registration.

This dataset is the first of its kind and the images can be used for the evaluation of image registration techniques to improve image–guidance in spinal surgery. The simulated US images provide a gold standard ground–truth for the registration techniques while the spatially tracked US images give a more realistic view of the vertebrae. In addition, the simulated US images can be used as a guide to validate real–time US simulation methods that are used in some image registration techniques [15,16], as well as preoperative simulation and planning [17].

In light of the above facts, we implemented two patch-based rigid registration algorithms: one based-on NCC and the other based-on the Correlation Ratio (CR) [18–20]. The barrier method with the logarithmic barrier function was used as the optimization technique [21]. Then, 6000 registration problems were created on the proposed datasets. By applying the methods on the set of registration problems, 12000 registrations were performed to align the images and compare the performance of methods. Our results show that both methods were able to register CT and US images of the proposed datasets successfully.

Fig. 1 Canine vertebrae, with the vinyl tubing inserted through the cavities and the rubber O-rings between each vertebrae, prior to complete immersion into the gel.

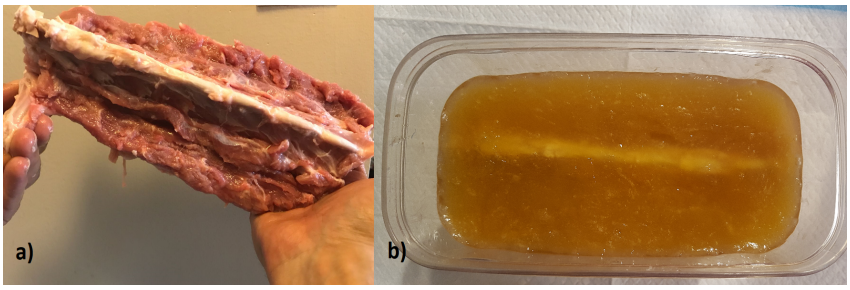

Fig. 2 The ex-vivo phantom. a) Lamb lumbar vertebrae before complete immersion into the gel and after removing the tissues over the dorsal midline. b) The lamb lumbar vertebrae in the gel phantom.

Table 1 Subjects' information

Patient	Dataset	Vertebrae Included	CT Scan	Intra-operative US	Simulated US
TCGA-QQ-ASV2	1	L1-L5	Yes	No	Yes
TCGA-QQ-ASVC	1	L1-L5	Yes	No	Yes
TCGA-QQ-A8VG	1	L1-L5	Yes	No	Yes
Canine Phantom	2	C6-C7-T1-T2	Yes	Yes	Yes
Lamb Phantom	3	L2-L5	Yes	Yes	Yes

2 Acquisition and Validation Methods

2.1 Subjects

The first database consists of the CT images provided by The Cancer Genome Atlas Sarcoma (TCGA-SARC) [13,14]. Patients were imaged with the CT scanner (GE LightSpeed VCT) using the protocol 5.7 CAP STANDARD-3CC/SEC. The axial slices had a thickness of $5.00mm$ and an in-slice resolution of $0.74 \times 0.74mm^2$. We extracted the lumbar vertebrae of the three patients with ID numbers TCGA-QQ-ASV2, TCGA-QQ-ASVC, and TCGA-QQ-A8VG using the 3D Slicer software.

The second database consists of the canine thoracic and cervical vertebrae phantom data. The phantom gel was created using a mixture of water, Knox unflavored gelatin, sugar-free Metamucil psyllium fiber supplement [22], and a Rubbermaid Premium Dry Food Storage Canister to store the mixture. The canine spine model was formed using vinyl tubing, a wooden skewer, rubber O-rings, and 10 vertebrae, namely the section of the canine cervical vertebrae (C6-C7) and a section of the thoracic vertebrae (T1-T8). Figure 1 shows the canine vertebrae before having it immersed into the gel.

The third database consists of the lamb vertebrae phantom data. Lamb vertebrae are most similar to human vertebrae in both the lumbar and thoracic regions [23]. Herein, we acquired our data using the L1-L5 vertebrae for a lamb. To simulate the spinal surgery, we created a surgical cavity (hemilaminectomy) on the posterior side of the vertebrae, and we performed a dorsal midline incision and removed the soft tissue covering that area (Fig. 2a). A means for US imaging was created by immersing the lumbar vertebrae into a gel as using the methods described earlier (Fig. 2b). Table 1 shows the summary of the subjects.

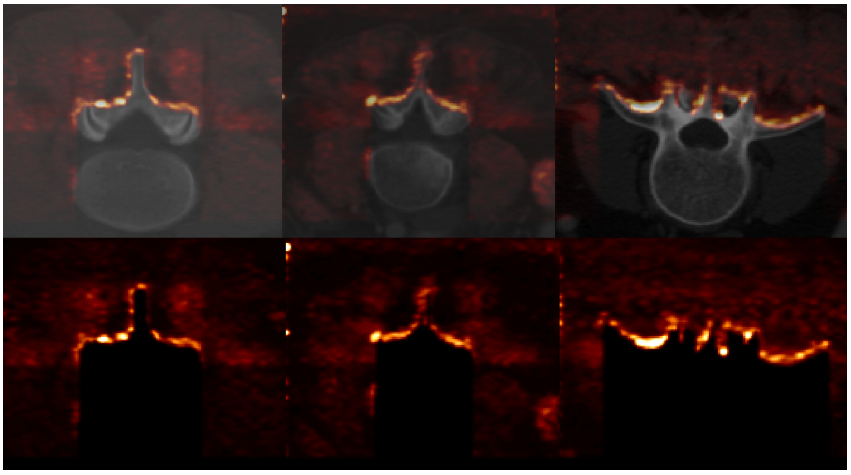

Fig. 3 Axial view of a slice of overlaying of US images on their corresponding CT images for Patient TCGA-QQ-ASV2 (column 1), Patient TCGA-QQ-ASVC (column 2), and Patient TCGA-QQ-ASVG (column 3) in the first row and simulated US images in the second row. US probe is located at the top of the image.

2.2 Simulation of US from CT

The Field II simulation software [24] was employed to simulate US images based on the CT scans. The simulated transducer assumes that the data was acquired with the patients lying in the prone position with the probe being perpendicular to the patients' back. The transducer consists of 192 elements with 64 active elements at a time having a frequency of 3.6 MHz and a propagation speed of 1540 m/s. The Field II simulation generated 50 raw radio-frequency (RF) lines of data from 10,000 scatterers. Each scatterer point is randomly located in a continuous space from the corresponding interpolated CT image where a Gaussian noise was added with a mean of zero and unit variance as its parameters.

After generating simulated RF signals, 2D B-mode US images were created from the RF data, followed by reconstruction of 3D volumes. Furthermore, the constructed volumetric image was resampled to the resolution of the CT volumetric image and as a result, the US and CT images were aligned by construction.

The simulator does not simulate shadowing artifacts of US below the bone surface. Hence, the CT volumetric image was used as a template to correct the US image. Similar to [10], forward ray-tracing followed by backward ray-tracing were used to extract the bone surfaces from the CT image. In the forward (backward) ray-tracing, the transducer radiates the sound waves through the CT images from anterior to posterior direction (posterior to anterior direction) and when they reach tissues with intensities of T or larger, it identifies the tissue as the bone surface. Consequently, the rest of the image in the wave's direction would appear as a dark shadow. The value of T was set to 150 Hounsfield in [10] given the acquired datasets. By inspecting the bone surfaces in the CT volumes in our datasets, we found that $T = 270$ is the optimal value. Finally, the processed CT volumetric image was multiplied voxel-wise to the US volumetric image as a mask. Figure 3 shows a slice of the simulated US images in the first row and, the second row displays the slice of the simulated US image overlaid on their corresponding CT image. The texture of the simulated US images is similar to real US images because they show the bone surfaces as back–scatters from the US wave. It is important to note that there are shadows below the bone surfaces where the US wave could not penetrate the tissues. Inherently co-registered, the aligned CT and US images make a gold standard ground-truth to validate image registration algorithms.

2.3 CT Scan Imaging

The phantom CT scan was acquired at Concordia University's PERFORM Centre in Montreal, Canada using a GE Discovery PET/CT 690 (Waukesha, WI) scanner with a 7.4 90000133 L-Spine Survey Helical protocol. The CT image has $0.351 \times 0.351 mm^2$ in-slice resolution and $0.625mm$ of slice thickness. The CT scan was executed so that the patients remained in the prone position with the orientation of the head facing the machine. The CT scan was acquired for the canine phantom and the lamb lumbar vertebrae.

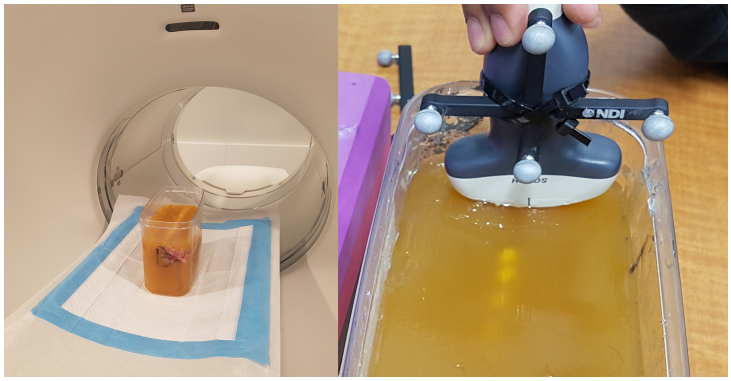

Fig. 4 Imaging the lamb vertebrae phantom. Acquiring CT scan (left) and tracked US (right).

2.4 Ultrasound Imaging

Following the CT scan, we immediately acquired the spatially tracked US image of the canine and lamb phantoms to minimize potential deformations of the models. The US images were acquired with an Alpinion E-CUBE 12R ultrasound machine (Bothell, WA) at the PERFORM Centre. The SC1-4H curvilinear 2D phase array transducer was set to a frequency of 4.0 MHz and a depth of 10.0 cm. Prior to the data acquisition, the probe was calibrated by N.M. at the PERFORM Centre using the PLUS Toolkit [25]. The probe was calibrated according to the method elaborated in [26]. The RMSE of $0.2mm$ and $3.7mm$ has been achieved for the pivot and US probe calibration. As it was explained in [26], The RMSE does not reflect the true error of calibration. There are some situations where the accuracy of calibration improves while the RMSE increases. The best way to verify the calibration is the qualitative validation, so the calibrations were validated by N.M.. The US images were tracked with Northern Digital Inc. (NDI, Waterloo, ON) Polaris camera and NDI passive reflective markers. The US images were recorded with the Epiphan Systems Inc. DVI2USB3.0 using the PLUS Toolkit [25], OpenIGTLink and the 3D Slicer as the acquisition software. Figure 4 shows the acquisition of the CT scan on the left side of the figure, and the acquisition of the spatially tracked US on the right of the figure.

2.5 Landmark Selection for Validation

For each of the canine and lamb phantom, two sets of 21 landmark pairs based on homologous structures between the CT and US images were selected. Each set of landmarks were independently selected by N. M. and C. B. using the 'register' software which is a part of the MINC Toolkit (https://bic-mni.github.io). The first 16 landmarks were used for the fiducial registration and the remaining landmarks for the evaluation of registration. Clear points of reference in each vertebra's surface structure such as inferior facet, superior facet, spinous process, transverse process were used to accurately select landmarks. We performed fiducial registration on each set of landmarks using a full affine transformation through the 3D Slicer software (https://www.slicer.org) and then resampled the US volumetric image to the CT volumetric image on each set of landmarks. We obtained Fiducial Registration Errors (FREs) of $3.5mm$ and $3.8mm$ for the first set of landmarks (selected by N. M.) of the canine and lamb phantom respectively and FREs of $1.3mm$ and $0.9mm$ for the second set of landmarks (Selected by C. B.) of the canine and lamb phantom respectively. As a result of the registration, the US and CT images were aligned with a silver standard ground truth. In order to validate the registration, using the last 5 landmarks, the FRE of less than $0.1mm$ was achieved for the canine and lamb phantom case. The set of 21 landmark pairs with FREs of $1.3mm$ and $0.9mm$ were provided in the database for the canine and lamb phantom respectively. Figure 5, shows axial view of intra-operative US and simulated US of the canine phantom C8 vertebra in the first and second rows respectively. From the left column, the figure shows CT, US, and overlaid CT-US respectively.

Figure 6 demonstrates the CT, US, and overlaid CT-US images of lumbar vertebrae the lamb in columns one, two, and three respectively. The rows show the sagittal view of intra-operative US and simulated US respectively. Table 2 shows the summary of landmark selection for canine phantom case and lamb lumbar vertebrae case.

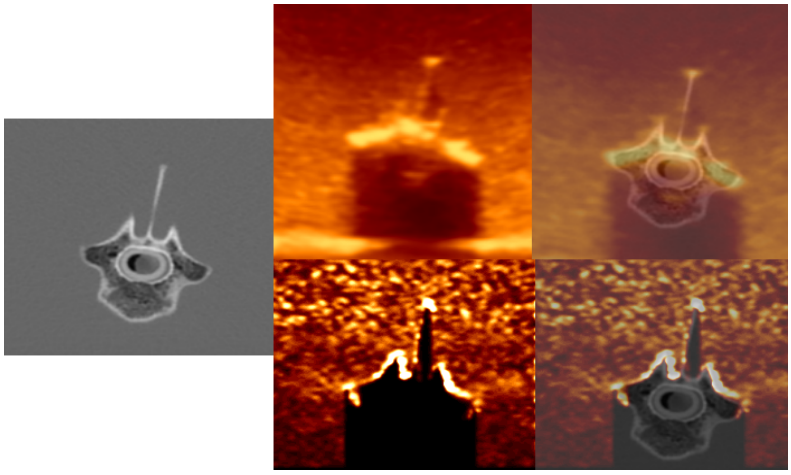

Fig. 5 Axial view of intra-operative US and simulated US of the canine phantom C8 vertebra in the first and second rows respectively. From the left column, the figure shows CT, US, and overlaid CT-US respectively.

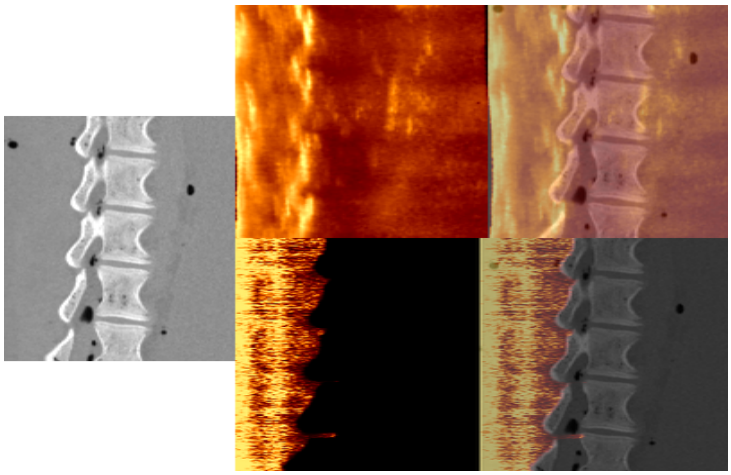

Fig. 6 The sagittal view of the lamb lumbar vertebrae. The first row shows the intraoperative US and the second row shows the simulated US. Columns from the left to the right show CT, US, and overlaid US on the CT image respectively.

Table 2 Summary of landmark selection

Subject	Number of Landmarks	FRE for Rater 1	FRE for Rater 2
Canine Phantom	16	3.52mm	1.31mm
Lamb Phantom	16	3.82mm	0.93mm

2.6 Data Format and Usage Notes

All images are provided with NIFTI and MINC formats. The first dataset can be used immediately after loading NIFTI or MINC images and the CT scans and simulated US images are aligned with a gold-standard ground-truth. The second and third datasets (the canine phantom and the lamb phantom) contain the CT scan, the intraoperative US, and the simulated US. For the CT scans and intraoperative US, 21 landmarks in MNI tag files are included so that they are aligned with a silver standard ground-truth and can also be used immediately after loading the NIFTI or MINC files. The CT scans and simulated US are aligned with a gold standard ground-truth. The data and the code are available at **https://doi.org/10.5281/zenodo.2652540** and **https://github.com/nimamasoumi/CT-US-Registration** respectively. Potential application of the dataset is elaborated in Section S1.

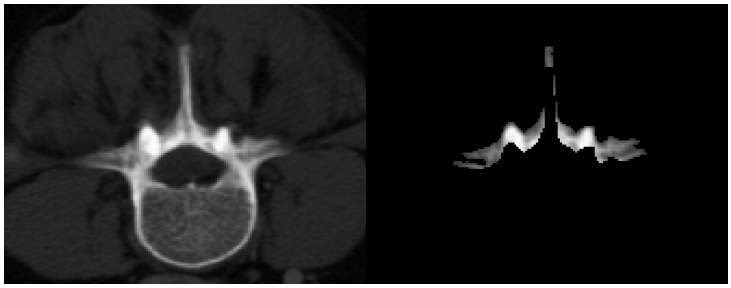

Fig. 7 Axial view of a CT image (left) and its corresponding extracted bone surface (right).

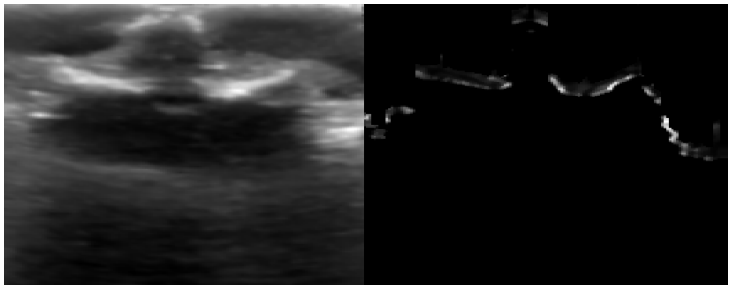

Fig. 8 Axial view of an intra-operative US image (left) and its corresponding extracted bone surface (right).

2.7 Pre-processing of CT and US for Registration

The CT and US images have different modalities and show different features of the rendered tissues. By inspecting the images, one might notice that in both modalities, the vertebral surface have rather high intensity compared to the other features in the images. Therefore by extracting the common features which are the bone surfaces in both volumes, the image registration will be facilitated.

The bone surface extraction in the images are based-on the method explained in [10] which is originally based- on [27]. Instead of applying the backward ray-tracing directly on the US images [10], it was applied on the gradient of US image from top to bottom in the axial view followed by a 3D median filter to remove some outliers. A slice of a pre-processed CT and US were demonstrated in Fig. 7 and Fig. 8 respectively. It is worth to mention that, the US pre-processing was only applied to the real US images and the simulated US images were utilized directly in the registration process.

2.8 Registration Methods

Two different registration methods were implemented and later in this paper were compared. Both methods are rigid registration using interior-point optimization technique, namely the barrier method [21]. The formulation of transformation is provided in Section S2.

2.8.1 Similarity Metrics

Two different similarity metrics were employed to evaluate the dissimilarity of corresponding $7 \times 7 \times 7$ patches of images. The patches are selected randomly and the number of patches have a direct relationship on the area of bone surfaces in the US images. The first method is based-on the normalized Cross-Correlation (NCC). Given the fact that the registration is pair-wised, if a patch of the moving image is Y and a patch of the fixed image is X, the calculation of NCC over the N_P number of patches is as Eq. 1, 2:

$$D_{NCC}(Y, X) = \frac{1}{N_p} \sum_{i=1}^{N_p} (1 - |\psi(Y, X; \boldsymbol{\Omega_i})|) \tag{1}$$

$$\psi(Y, X) = \frac{\sum(Y.X)}{\sqrt{\sum Y^2}.\sqrt{\sum X^2}} \tag{2}$$

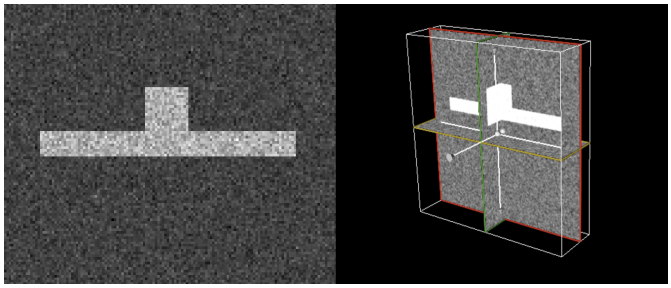

Fig. 9 Axial view of the synthetic volume (left) and the 3D view (right).

where $|\cdot|$ operator takes the absolute value. The second dissimilarity matrix is based on the Correlation Ratio and it was elaborated in [19]. The Eq. 3, 4, 5 are the CR equations as it was used in the optimization.

$$D_{CR}(Y,X) = \frac{1}{N_p}\sum_{i=1}^{N_p}(1-\eta(Y|X;\boldsymbol{\Omega_i})) \tag{3}$$

$$1-\eta(Y|X) = \frac{1}{N\sigma^2}\left(\sum_{t=1}^{N} Y_t^2 - \sum_{j=1}^{N_b} N_j\mu_j^2\right) \tag{4}$$

$$\mu_j = \frac{\sum_{t=1}^{N}\lambda_{t,j}Y_t}{N_j}, N_j = \sum_t \lambda_{t,j} \tag{5}$$

where $\lambda_{t,j}$ is the contribution of sample t to bin j in X, N is the total number of samples in a patch, and $\sigma^2 = Var[Y]$ is the variance of patch.

2.8.2 Optimization Technique

The barrier method [21] was employed to find the optimal rigid transformation which minimizes the D_{NCC} and D_{CR} in Eq. 1 and Eq. 3 respectively. The natural logarithm was set as the barrier function using the multi-scale pyramid processing to estimate larger displacements. In the finest to most coarse resolution, maximum number of 15, 50, and 100 iterations were used (three levels).

3 Results

In the pre-processing, the bone surface of the CT images are extracted and they are already registered to the simulated US images as well as the real US images. In the following, the images are misaligned and using the registration methods, they were reregistered.

3.1 Synthetic Data

Figure 9 shows the synthetic volume created by MATLAB. This volume was created to register to itself later in the experiments. Brighter part of the image has a range of intensities with additive Gaussian noise. The volume has general similarities to the bone surface extracted from the CT images and the US images. Registration of synthetic volume to itself is the simplified version of registering the bone surface extracted from the CT images to the US images.

3.2 Registration Problems

Given the fact that the CT images and the US images are pre-registered and aligned, in order to evaluate the registration methods described in Section 2.8.1, first the images are required to be misaligned. Therefore, 100 different registration problems were created for each misalignment intervals of $0-2$ voxels (vox), $2-4vox$, $4-6vox$, $6-8vox$, $8-10vox$, and $10-12vox$ which gives the total number of 600 registration problems for each pairs of images. Each misalignment problem was created by only rotation

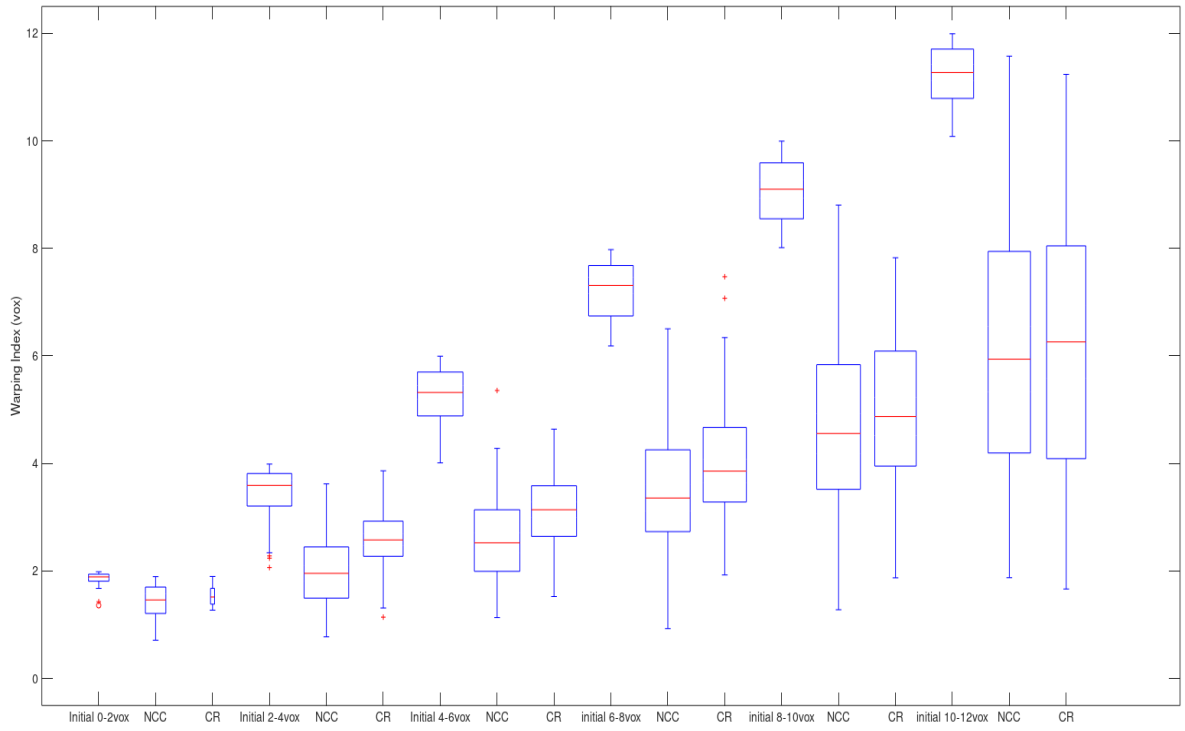

Fig. 10 Comparison of NCC and CR methods in registration of the CT and intraoperative US of the Canine Phantom.

and the translation of images. The pairs which are selected to be misaligned and then registered are synthetic data to itself, CT to the simulation US of the subject TCGA-QQ-ASV2, CT to the simulation US of the subject TCGA-QQ-ASVC, CT to the simulation US of the subject TCGA-QQ-A8VG, CT to the simulation US of the Canine Phantom, CT to the intraoperative US of the subject the Canine Phantom, CT to the simulation US of the Lamb Phantom part 1, CT to the simulation US of the Lamb Phantom part 2, CT to the intraoperative US of the subject the Lamb Phantom part1, and CT to the intraoperative US of the subject the Lamb Phantom part 2. Note that the Lamb phantom volumes had almost twice number of slices than the other volumes and was divided into roughly two equal parts for the speed and the simplicity of registration problems.

3.3 Registration Procedure

Having the pairs of images in the Section 3.2 (total 10 pairs), the pre-processed CT images and the corresponding US pairs are passed to the misalignment unit. In our experiments, the pre-processed CT is fixed and the corresponding US pair was misaligned. Then the misaligned US pair is pre-processed (only for the intraoperative US) and then passed through the registration unit. The registration unit estimates a rigid transformation which aligns the images and passes the transformation to the validation unit. The validation unit compares the warping index before and after the registration.

3.4 Succes Rate and Box Plots

The success rate is the number of registration problems which the methods could decrease the warping index for each pair and each error (misalignment) interval over the total number of registration for that pair and that interval (which is 100 for all intervals and pairs here). The following box plots are comparing the CR and NCC for each pair in registration problems where the methods could decrease the warping index. Figure 10 is the result of registration for the CT and intraoperative US of the Canine Phantom. Figure 11 shows the success rate for the corresponding pair. In these pairs, NCC outperformed CR in both decreasing the warping index and having better success rate. The detailed results for the rest of subjects are provided in Section S3.

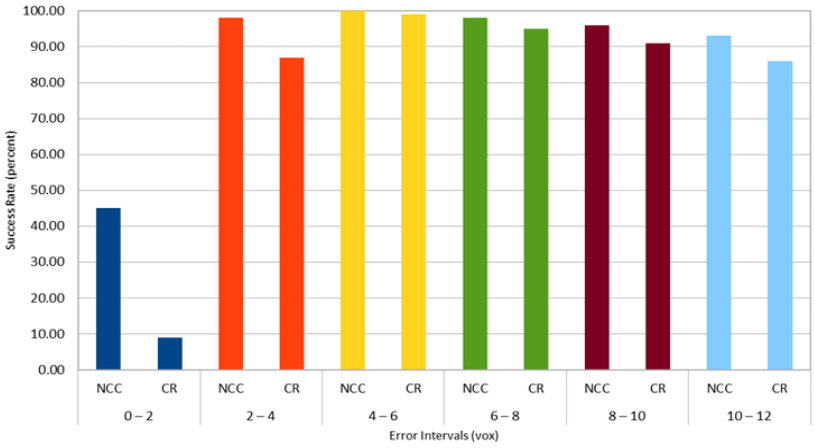

Fig. 11 Success rate of the registration of CT and intraoperative US of the Canine Phantom for the NCC and CR.

4 Discussions

In Section 2.2, a method was elaborated to produce simulated US images using the Field II package [24]. Since this package does not allow modeling the full reflection of the wave at the bone surface, we set the scatterer intensities below the bone surface to zero. This creates sharp edge artifacts at the bone surface, which can be considered as a limitation of this database.

The NCC registration method could show better performance in the registration problems where real US image is involved while the CR generally had better performance where simulated US images are registered to the CT images. The registration algorithms were executed in a machine with 4 CPU workers and a machine with 12 CPU workers. Obviously the registrations that were implemented by the 12 CPU workers were 2 to 3 times faster. The NCC method was implemented in MATLAB (MathWorks, Inc., Natick, USA), and the CR implementation was in MATLAB and C++ to decrease the execution time of image binning.

In the small error intervals, especially $0 - 2vox$, compared to NCC, CR did not have good success in the alignment of CT and intra-operative US images. One reason is that both Canine Phantom and the Lamb Phantom have pre-existing initial misalignment even after fiducial registration. This may leave CR method with no improvement of the alignment which reduces the success rate.

5 Conclusion

Herein, a database of CT, intraoperative US, and simulated US were presented. This database consists of 3 datasets and in total 5 subjects. For each subject, the simulated US from CT was provided. The database provides a resource for evaluating image registration techniques. The simulated data have two applications. First, they provide the gold standard ground–truth which is difficult to obtain with ex–vivo and in–vivo data for validating US–CT registration methods. Second, the simulated US images can be used to validate real–time US simulation methods, since our database is simulated using the computationally expensive but physically realistic Field II package. Two patch-based rigid image registration methods were implemented to register the CT and US images after misaligning them. The methods are employing NCC and CR as the similarity metrics and the barrier method to optimize similarity of images. The results of registration show that the methods were successful in aligning the pre-processed CT and US images by decreasing the warping index. Given this fact, the proposed image registration techniques can be useful to potentially improve ultrasound-guided interventions of the spine.

Acknowledgements This work was supported in part by the Natural Sciences and Engineering Research Council of Canada (NSERC) and in part by the Regroupment Strategique en Microelectronique du Quebec.

6 Compliance with Ethical Standards

Conflict of interest The authors declare that there is no conflict of interest.

Ethical standard All procedures performed in studies involving human participants were in accordance with the ethical standards of the institutional and/or national research committee and with the 1964 Declaration of Helsinki and its later amendments or comparable ethical standards.
Informed consent Informed consent was obtained from all participants included in the study.

References

1. I. J. Gerard, M. Kersten-Oertel, S. Drouin, J. A. Hall, K. Petrecca, D. De Nigris, D. A. Di Giovanni, T. Arbel, and D. L. Collins, "Combining intraoperative ultrasound brain shift correction and augmented reality visualizations: a pilot study of eight cases," *Journal of Medical Imaging*, vol. 5, no. 2, p. 021210, 2018.
2. G. M. Della Pepa, G. Sabatino, C. L. Sturiale, E. Marchese, A. Puca, A. Olivi, and A. Albanese, "Integration of real-time intraoperative contrast-enhanced ultrasound and color doppler ultrasound in the surgical treatment of spinal cord dural arteriovenous fistulas," *World Neurosurgery*, vol. 112, pp. 138–142, 2018.
3. M. Ganau, N. Syrmos, A. R. Martin, F. Jiang, and M. G. Fehlings, "Intraoperative ultrasound in spine surgery: history, current applications, future developments," *Quantitative imaging in medicine and surgery*, vol. 8, no. 3, p. 261, 2018.
4. J.-F. Boursier, A. Fournet, J. Bassanino, M. Manassero, A.-S. Bedu, and D. Leperlier, "Ultrasonography is more accurate than percutaneous palpation for identifying targeted thoracolumbar intervertebral disc spaces in dogs," *Veterinary Radiology & Ultrasound*, 2018.
5. W. Wein, S. Brunke, A. Khamene, M. R. Callstrom, and N. Navab, "Automatic ct-ultrasound registration for diagnostic imaging and image-guided intervention," *Medical image analysis*, vol. 12, no. 5, pp. 577–585, 2008.
6. O. Mattausch and O. Goksel, "Image-based reconstruction of tissue scatterers using beam steering for ultrasound simulation," *IEEE transactions on medical imaging*, vol. 37, no. 3, pp. 767–780, 2018.
7. M. Tuzer, R. Türkay, M. Boyman, and B. Acar, "Multi-ray medical ultrasound simulation without explicit speckle modelling," *International journal of computer assisted radiology and surgery*, pp. 1–9, 2018.
8. P. Rubi, E. F. Vera, J. Larrabide, M. Calvo, J. D'Amato, and I. Larrabide, "Comparison of real-time ultrasound simulation models using abdominal ct images," in *12th International Symposium on Medical Information Processing and Analysis*, vol. 10160, p. 1016009, International Society for Optics and Photonics, 2017.
9. B. Burger, S. Bettinghausen, M. Radle, and J. Hesser, "Real-time gpu-based ultrasound simulation using deformable mesh models," *IEEE transactions on medical imaging*, vol. 32, no. 3, pp. 609–618, 2013.
10. C. X. Yan, B. Goulet, J. Pelletier, S. J.-S. Chen, D. Tampieri, and D. L. Collins, "Towards accurate, robust and practical ultrasound-ct registration of vertebrae for image-guided spine surgery," *International journal of computer assisted radiology and surgery*, vol. 6, no. 4, pp. 523–537, 2011.
11. T. K. Koo and W. E. Kwok, "Hierarchical ct to ultrasound registration of the lumbar spine: a comparison with other registration methods," *Annals of biomedical engineering*, vol. 44, no. 10, pp. 2887–2900, 2016.
12. Y. Xiao, M. Fortin, G. Unsgård, H. Rivaz, and I. Reinertsen, "Retrospective evaluation of cerebral tumors (resect): A clinical database of pre-operative mri and intra-operative ultrasound in low-grade glioma surgeries," *Medical physics*, vol. 44, no. 7, pp. 3875–3882, 2017.
13. K. Clark, B. Vendt, K. Smith, J. Freymann, J. Kirby, P. Koppel, S. Moore, S. Phillips, D. Maffitt, and M. Pringle, "The cancer imaging archive (tcia): maintaining and operating a public information repository," *Journal of digital imaging*, vol. 26, no. 6, pp. 1045–1057, 2013.
14. C. Roche, E. Bonaccio, and J. Filippini, "Radiology data from the cancer genome atlas sarcoma [tcga-sarc] collection," *The Cancer Imaging Archive*, 2016.
15. A. Karamalis, W. Wein, and N. Navab, "Fast ultrasound image simulation using the westervelt equation," in *International Conference on Medical Image Computing and Computer-Assisted Intervention*, pp. 243–250, Springer, 2010.
16. S. Gill, P. Abolmaesumi, G. Fichtinger, J. Boisvert, D. Pichora, D. Borshneck, and P. Mousavi, "Biomechanically constrained groupwise ultrasound to ct registration of the lumbar spine," *Medical image analysis*, vol. 16, no. 3, pp. 662–674, 2012.
17. J. Jaros, A. P. Rendell, and B. E. Treeby, "Full-wave nonlinear ultrasound simulation on distributed clusters with applications in high-intensity focused ultrasound," *The International Journal of High Performance Computing Applications*, vol. 30, no. 2, pp. 137–155, 2016.
18. A. Roche, G. Malandain, X. Pennec, and N. Ayache, "The correlation ratio as a new similarity measure for multimodal image registration," in *International Conference on Medical Image Computing and Computer-Assisted Intervention*, pp. 1115–1124, Springer, 1998.
19. H. Rivaz, S. J.-S. Chen, and D. L. Collins, "Automatic deformable mr-ultrasound registration for image-guided neurosurgery," *IEEE transactions on medical imaging*, vol. 34, no. 2, pp. 366–380, 2015.
20. N. Masoumi, Y. Xiao, and H. Rivaz, "Arena: Inter-modality affine registration using evolutionary strategy," *International journal of computer assisted radiology and surgery*, vol. 14, no. 3, pp. 441–450, 2019.
21. S. Boyd, S. P. Boyd, and L. Vandenberghe, *Convex optimization*. Cambridge university press, 2004.
22. J. L. Kendall and J. P. Faragher, "Ultrasound-guided central venous access: a homemade phantom for simulation," *Canadian Journal of Emergency Medicine*, vol. 9, no. 5, pp. 371–373, 2007.
23. H.-J. Wilke, A. Kettler, K. H. Wenger, and L. E. Claes, "Anatomy of the sheep spine and its comparison to the human spine," *The Anatomical Record: An Official Publication of the American Association of Anatomists*, vol. 247, no. 4, pp. 542–555, 1997.
24. J. A. Jensen, "Field: A program for simulating ultrasound systems," in *10th nordicbaltic conference on biomedical imaging, vol. 4, supplement 1, part 1: 351–353*, Citeseer, 1996.
25. A. Lasso, T. Heffter, A. Rankin, C. Pinter, T. Ungi, and G. Fichtinger, "Plus: open-source toolkit for ultrasound-guided intervention systems," *IEEE Transactions on Biomedical Engineering*, vol. 61, no. 10, pp. 2527–2537, 2014.
26. T. Ungi, A. Lasso, and G. Fichtinger, "Open-source platforms for navigated image-guided interventions," *Medical Image Analysis*, vol. 33, pp. 181–186, 2016.
27. B. Brendel, S. W. A. Rick, M. Stockheim, and H. Ermert, "Registration of 3d ct and ultrasound datasets of the spine using bone structures," *Computer Aided Surgery*, vol. 7, no. 3, pp. 146–155, 2002.